arXiv:cond-mat/0506732v1 [cond-mat.supr-con] 28 Jun 2005

Modern Physics Letters B
© World Scientific Publishing Company

MECHANISM OF HIGH-T_c SUPERCONDUCTIVITY BASED MAINLY ON TUNNELING MEASUREMENTS IN CUPRATES*

A. MOURACHKINE

Cavendish Laboratory, University of Cambridge, Madingley Road, Cambridge, CB3 0HE, UK
andrei_mourachkine@yahoo.co.uk

Received June 2005

The main purpose of this *brief* review is to present a sketch of the mechanism of high-T_c superconductivity based mainly on tunneling measurements in cuprates. In the review, we shall mostly discuss tunneling *spectroscopy* in $Bi_2Sr_2CaCu_2O_8$. Analysis of the data shows that the Cooper pairs in cuprates are topological excitations (e.g. quasi-one dimensional bisolitons, discrete breathers etc.), and the phase coherence among the Cooper pairs appears due to spin fluctuations.

Keywords: Cuprates; tunneling; mechanism of high-T_c superconductivity.

PACS Number(s): 74.50.+r, 74.72.-h, 74.62.Dh, 72. 20.-z, 72.25.Dw

1. Introduction

Superconductivity (SC) discovered in 1911 by Kamerlingh Onnes[1] and his assistant Holst has remained a major scientific mystery for a large part of the last century. It was completely understood only in 1957 when Bardeen, Cooper and Schrieffer (BCS) formulated the microscopic theory of SC in metals.[2] The central concept of the BCS theory is the weak electron-phonon interaction which leads to the appearance of an attractive potential between two electrons. As a consequence, some electrons form pairs, and thus, composite bosons. The long-range phase coherence among the pairs appears due to the overlap of their wavefunctions, leading to a peculiar correlated state of matter—a quantum state on a macroscopic scale, in which all the electron pairs move in a single coherent motion.

In 1986, Bednorz and Müller found SC in La-Ba-Cu-O ceramics at 30 K.[3] In 1993, the maximum critical temperature of copper oxides (cuprates) reached 135 K. The crystal structure of cuprates is layered and highly anisotropic. The parent compounds of SC cuprates are antiferromagnetic (AF) Mott insulators. A Mott insulator has a charge gap of ~ 2 eV, whereas the spin wave spectrum extends to

*This brief review is based on the talk given at the University of Cambridge in May 2004, and the talk, in its turn, is based on a book (Ref. 6).

zero energy. When cuprates are slightly doped by holes or electrons, on cooling they become SC. The doped carriers are accumulated in two-dimensional CuO_2 planes. Thus, for SC in cuprates, the carrier density in CuO_2 planes is the main factor. SC occurs at low temperatures when the doping level is approximately one doped carrier per three Cu^{2+} ions ($\sim 16\%$).

Soon after the discovery of high-T_c superconductivity (HTSC), it became clear that the concept of the Fermi liquid is not applicable to cuprates: the normal state properties of cuprates are markedly different from those of conventional metals. A normal-state partial gap, the pseudogap (PG), appearing in electronic excitation spectra of cuprates above T_c, is one of the main features of HTSCs.[4] There is an interesting contrast between the development of the physics of cuprates and that of the physics of conventional SCs. Just before the creation of the BCS theory, the normal-state properties of conventional metals were very well understood; however SC was not. The situation with the cuprates was just the opposite: at the time HTSC was discovered, there already existed a good understanding of the phenomenon of SC, but the normal-state properties of cuprates were practically unknown.

In addition to their peculiar normal-state properties, several experiments show that some SC properties of cuprates deviate from predictions of the BCS theory. For example, the isotope effect is almost absent in *optimally* doped cuprates.[5,6,7] Thus, on a microscopic scale, there is a clear difference between conventional SCs and HTSCs, namely that they have a different origin and that different criteria are required for HTSCs than for classical SCs. In the absence of a commonly accepted theory of HTSC, it is still time to discuss experimental data obtained in cuprates.

The main purpose of this brief review is to present a more or less coherent picture of the mechanism of HTSC based mainly on tunneling measurements in cuprates. In the review, we shall focus our attention on hole-doped cuprates. We shall mainly discuss tunneling *spectroscopy* in $Bi_2Sr_2CaCu_2O_8$ (Bi2212) performed by the present author. We shall also use some inelastic neutron scattering (INS) and muon spin resonance (μSR) data. The main ideas of the review appeared in 1998.[8] Since the review is based on experimental data, the reader will not find many formulas in the text, not a single Hamiltonian. *Due to the restriction on the number of pages in a review, only limited number of experimental data can be presented here.* More tunneling data and a more detailed description of the mechanism of HTSC based on the data can be found elsewhere.[6,7]

Analysis of the data shows that (i) there are two SC gaps in cuprates: a pairing and a phase coherence gap. (ii) Tunneling spectra below T_c are a combination of coherent QP peaks and incoherent part from a normal-state PG. (iii) The "tunneling" normal-state PG is most likely a charge gap. (iv) However, SC cuprates have the second normal-state PG which is magnetic and, most likely, spatially separated from the charge PG. (v) Just above T_c, incoherent Cooper pairs contribute to the "tunneling" PG. (vi) There is a clear correlation between the magnitude of pairing gap and the magnitude of "tunneling" PG in Bi2212 ($\Delta_p \simeq \Delta_{pg}/3$). (vii) Tunneling

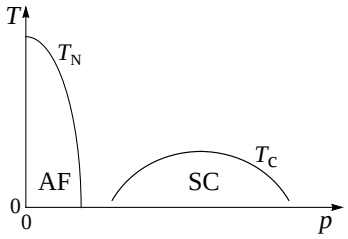

Fig. 1. Phase diagram of hole-doped cuprates: AF and SC phases. T_N is the Néel temperature, and p is the hole concentration into the CuO_2 planes.

characteristics corresponding to the SC condensate are in good agreement with theoretical predictions for topological excitations (solitons). (viii) In addition, analysis of INS and μSR data shows that the long-range phase coherence occurring at T_c is established due to spin fluctuations into CuO_2 planes.

2. Starting Point: Phase Diagram of Cuprates

Let us start the review with the "basics," i.e. with what is widely accepted. Figure 1 shows a sketch of phase diagram of hole-doped cuprates. At low doping level, cuprates are AF. The SC state occurs at higher hole concentrations in CuO_2 planes. If in $La_{2-x}Sr_xCuO_4$ (LSCO), there is a distance between the AF and SC phases, in $YBa_2Cu_3O_7$ (YBCO), the SC state practically evolves from the AF phase.

In conventional SCs, the critical temperature rises monotonically with the rise of charge-carrier concentration, $T_c(p) \propto p$, where p is the carrier concentration. In cuprates, the $T_c(p)$ dependence is nonmonotonic. In hole-doped cuprates, the $T_c(p)$ dependence has a bell-like shape and, in most of them, can be approximated by the empirical expression $T_c(p) \simeq T_{c,max}[1 - 82.6(p - 0.16)^2]$, where $T_{c,max}$ is the maximum critical temperature for a given compound.[9] SC occurs within the limits $0.05 \leqslant p \leqslant 0.27$ which vary slightly in different cuprates. Different doping regions of the SC phase are mainly known as *underdoped* ($0.05 \leqslant p \leqslant 0.14$), *optimally doped* ($0.14 < p < 0.18$) and *overdoped* ($0.18 \leqslant p \leqslant 0.27$). The insulating phase at $p < 0.05$ is usually called the *undoped* region. Above $p = 0.27$, cuprates are practically metallic. The state above the SC dome is often called a strange metal. Paradoxically, the $T_{c,max}$ in cuprates is located near $p = 0.16$, whereas the SC condensation energy has the maximum in the overdoped region near $p = 0.19$.[10]

The PG, a normal-state partial gap appearing in electronic excitation spectra of cuprates above T_c, is not shown in Fig. 1. The reason is very simple: there is no agreement on the *exact* doping dependence of the PG. In spite of the fact that there is a consensus on *general* doping dependence of the PG in hole-doped cuprates—the magnitude of the PG decreases with increase of hole concentration—however, there is a clear discrepancy between the phase diagrams inferred from transport, nuclear magnetic resonance (NMR) and heat-capacity measurements,

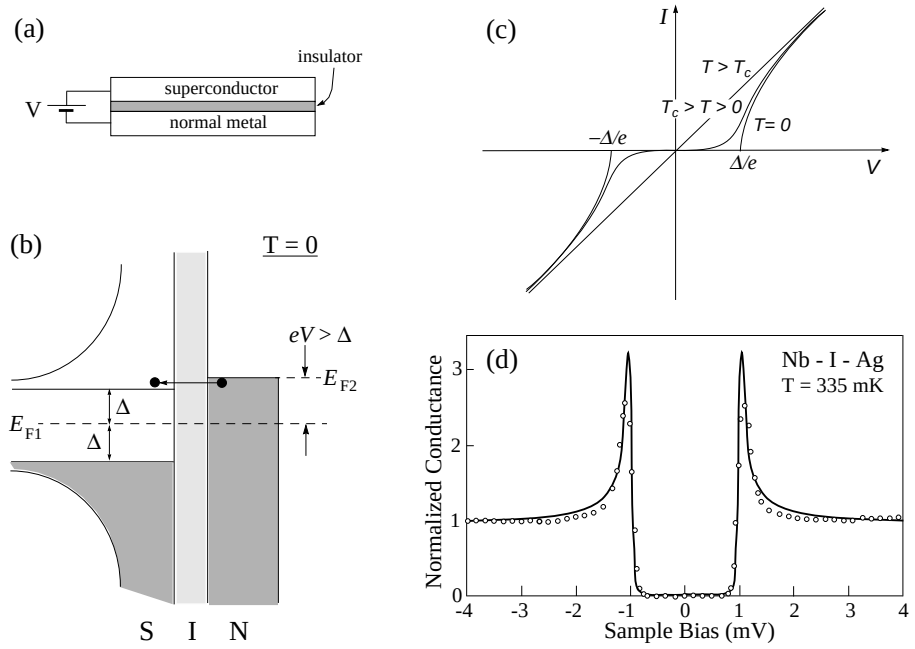

Fig. 2. (a) Sketch of an SIN tunneling junction, and (b) corresponding energy diagram at $T = 0$ in the presence of an applied voltage: QPs can tunnel when $|V| \geq \Delta/e$. (c) Tunneling $I(V)$ characteristics for an SIN junction at different temperatures: $T = 0$; $0 < T < T_c$, and $T > T_c$ (the latter case corresponds to a NIN junction). At $0 < T < T_c$, QP excitations exist at any applied voltage. (d) Tunneling conductance (circles) versus sample bias obtained in a Nb-I-Ag junction at 335 mK.[11] The solid line is a theoretical curve calculated from Eqs. (3) and (2).

on one hand, and from tunneling measurements, on the other hand. Transport, NMR and heat-capacity measurements show that, in the overdoped region, the PG is absent above T_c. At the same time, in tunneling measurements, the PG is observed well above T_c. Generally speaking, the PG in cuprates may arise from charge-density waves (CDW), local AF correlations [or spin-density waves (SDW)], or from their combination. Incoherent Cooper pairs may also induce a PG. From the common sense, however, the PG is most likely a charge gap because, at low doping level, cuprates are AF Mott insulators and, therefore, a spin gap is absent at low p. Alternatively, there are two PGs in cuprates.

3. Tunneling Spectroscopy in Metals

The tunneling spectroscopy is a powerful tool, and has played a crucial role in the verification of the BCS theory.[6] Tunneling spectroscopy is particularly sensitive to the density of state (DOS) near the Fermi level, E_F, and, thus, is capable of detecting any gap in the quasiparticle (QP) excitation spectrum at E_F. In addition, it has a very high energy resolution: less than k_BT for SC-insulator-SC (SIS) junctions,

where k_B is the Boltzmann constant. In comparison with photoemission measurements, tunneling spectroscopy has an additional advantage: to measure the DOS locally.

3.1. *SIN tunneling*

Consider the flow of electrons across a thin insulating layer having the thickness of a few nanometers, which separates a normal metal from a conventional SC. Figure 2a shows a SC-insulator-normal metal (SIN) tunneling junction. At $T = 0$, no tunneling current can appear if the absolute value of the applied voltage (bias) in the junction is less than Δ/e. Tunneling will become possible when the applied bias reaches the value of $\pm\Delta/e$, as shown in Fig. 2b. Figure 2c shows schematically three current-voltage $I(V)$ characteristics for an SIN junction at $T = 0$, $0 < T < T_c$ and $T_c < T$. At $T = 0$, the absence of a tunneling current at small voltages constitutes an experimental proof of the existence of a gap in the energy spectrum of a SC. At $0 < T < T_c$, there are always excited electrons due to thermal excitations. As shown in Fig. 2c, the $I(V)$ curves, obtained below T_c, approach at high bias the $I(V)$ characteristic measured above T_c (i.e. Ohm's line). In conventional SCs, the gap completely vanishes at T_c. This, however, is not the case for cuprates which show the presence of a PG above T_c.

3.2. *Density of states*

In the framework of the BCS theory, the DOS of QP excitations in the SC state, $N_s(E)$, and the DOS in the normal state $N_n(E)$ relate to each other at $T = 0$ as

$$N_s/N_n = \begin{cases} \frac{E}{\sqrt{E^2-\Delta^2}} & \text{for } |E| \geq \Delta \\ 0 & \text{if } |E| < \Delta. \end{cases} \tag{1}$$

In most low-T_c SCs, N_n is normally constant over the energy range of interest.

A $dI(V)/dV$ tunneling characteristic obtained in an SIN junction corresponds directly to the DOS of QP excitations in a SC. In a first approximation, assuming that the normal metal has a constant DOS near the Fermi level and the transmission of the barrier (insulator) is independent of energy, the tunneling conductance $dI(V)/dV$ is proportional to the DOS of a SC, broadened by the Fermi function $f(E,T) = [\exp(E/k_BT) + 1]^{-1}$. Thus, at low temperature

$$\frac{dI(V)}{dV} \propto \int_{-\infty}^{+\infty} N_s(E) \left[-\frac{\partial}{\partial(eV)} f(E + eV, T) \right] dE \cong N_s(eV), \tag{2}$$

where e is the electron charge, and the origin of energy scale E in the tunneling spectra corresponds to the Fermi level of the SC. Consequently, the differential conductance at negative (positive) voltage reflects the DOS below (above) E_F.

In order to smooth the gap-related structures in the DOS $N_s \propto E/\sqrt{E^2 - \Delta^2}$, a phenomenological smearing parameter Γ was introduced, which accounts for a

lifetime broadening of QPs ($\Gamma = \hbar/\tau$, where τ is the lifetime of QP excitations).[12] The energy E in the DOS function is replaced by $E - i\Gamma$:

$$N_s(E,\Gamma) \propto Re\left\{\int \frac{E - i\Gamma}{\sqrt{(E - i\Gamma)^2 - (\Delta(\vec{k}))^2}} d\vec{k}\right\}, \tag{3}$$

where we introduced $\Delta(\vec{k})$ which is the $\vec{k}$-dependent energy gap for the general case of an anisotropic gap. In the two-dimensional case, the integration is reduced to the in-plane angle, $0 \leq \theta < 2\pi$.

In SIN tunneling junctions of conventional SCs, there is good agreement between the theory and experiment. As an example, Figure 2d shows the correspondence between experimental data obtained in Nb and the theoretical curve.

3.3. *SIS tunneling*

In an SIS junction, the tunneling conductance is proportional to the convolution of the DOS function of a SC with itself. In the case of symmetrical SIS contacts, the expression for the tunneling current through contacts at finite temperature is

$$I(V) = K \int_0^\infty N(E,\Gamma)N(E - eV,\Gamma)[f(E,T) - f(E - eV,T)]dE, \tag{4}$$

where K is the constant (matrix) which contains tunneling probabilities. The expression for tunneling conductance at finite temperature can be presented as

$$\frac{(dI/dV)_s}{(dI/dV)_n} = \frac{d}{d(eV)} \int_0^{eV} N(E,\Gamma)N(E - eV,\Gamma)[f(E,T) - f(E - eV,T)]dE, \tag{5}$$

where $(dI/dV)_n$ is the conductance in the normal state.

If, in SIN tunneling junctions of s-wave SCs, there is good agreement between the theory and experiment, as shown in Fig. 2d, in SIS junctions the correspondence between the BCS DOS and experimental data is poor (see p. 31 in Ref. 6).

4. Bi2212 Samples and Tunneling Techniques

Overdoped Bi2212 single crystals were grown by the self-flux method in Al_2O_3 and ZrO_2 crucibles and then mechanically separated from the flux. The dimensions of these crystals are typically 2–3×1×0.1 mm^3. The chemical composition of the Bi-2:2:1:2 phase in these single crystals corresponds to the formula $Bi_2Sr_{1.9}CaCu_{1.8}O_{8+x}$ as measured by energy dispersive X-ray fluorescence (EDX). The crystallographic a, b, c values are of 5.41, 5.50 and 30.81 Å, respectively. The T_c value was determined by the four-contact method yielding T_c = 87–90 K with the transition width less than 1 K. The underdoped Bi2212 single crystals were obtained by annealing the overdoped crystals in vacuum.

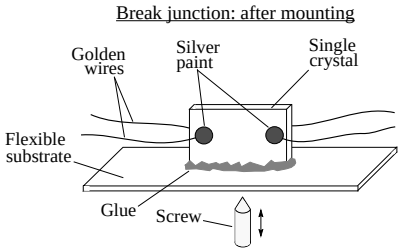

Fig. 3. Sketch of a BJ after mounting: a single crystal with four electrical contacts is glued to a flexible substrate. The crystal is broken by bending the substrate by a differential screw.

Bi2212 single crystals in which Cu is partially substituted for Ni or Zn were also grown by the self-flux method. As measured by EDX the chemical composition of the Bi-2:2:1:2 phase in Ni-doped and Zn-doped Bi2212 single crystals corresponds to the formula $Bi_2Sr_{1.95}Ca_{0.95}(CuNi)_{2.05}O_{8+x}$ and $Bi_2Sr_{1.98}Ca_{0.83}(CuNi)_2O_{8+x}$, respectively. In these single crystals the Ni and Zn content with respect to Cu was approximately 1.5% and 1%, respectively. The T_c value was determined by the four-contact method: $T_c = 75$–77 K in Ni-doped Bi2212 and $T_c = 76$–78 K in Zn-doped Bi2212. In both types of single crystals, the transition width is a few degrees.

Most tunneling data presented in this review were obtained by the break-junction (BJ) technique. Figure 3 schematically depicts the BJ setup. A single crystal is glued to a flexible insulating substrate, as shown in Fig. 3, such that the *ab* plane of the crystal is perpendicular to the substrate surface. Four electrical contacts (typically with a resistance of a few Ohms) are made by attaching gold wires to the crystal by silver paint. The diameter of golden wires is 25 μm. Two contacts situated diagonally are used for bias input, which is slightly modulated by a lock-in, and the other two for measuring $dI(V)/dV$ and $I(V)$ tunneling characteristics. At low temperature, the crystal is broken in an He ambient in the *ab* plane by bending the flexible substrate. The bending force is applied by the differential screw shown schematically in Fig. 3. The differential screw has a precision of 10 μm per turn. Tunneling is achieved by changing the distance between broken parts of the crystal. The $dI(V)/dV$ and $I(V)$ tunneling characteristics are determined by a standard lock-in modulation technique.

In one junction, a few tunneling spectra are usually obtained at low (constant) temperature by changing the distance between broken parts of a crystal, going back and forth etc., and each time the tunneling occurs most likely in different places.

In addition to SIS-junction measurements, tunneling tests have also been carried out in Bi2212 single crystals by forming SIN junctions. In point-contact measurements, the differential screw shown in Fig. 3 is used to push a normal tip against a fixed single crystal. Pt-Ir and Ag wires sharpened mechanically were used as normal tips. The point-contact measurements were performed either along or perpendicular to the *c* crystal axis.

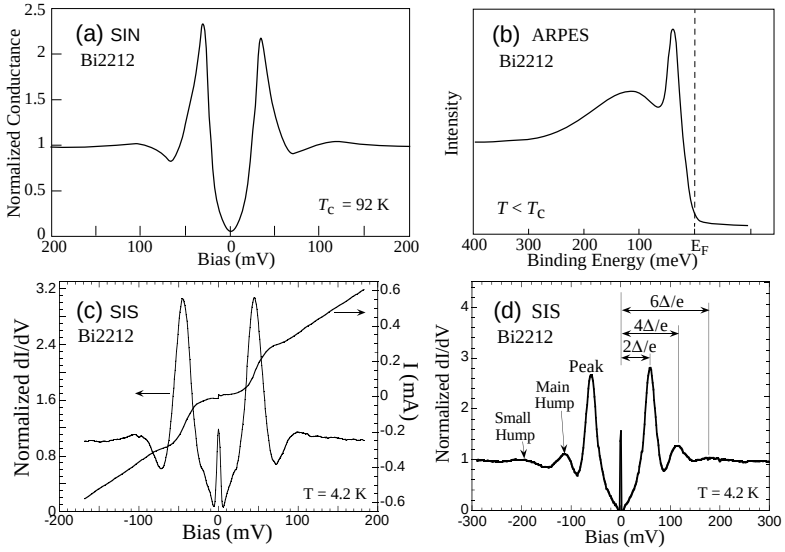

Fig. 4. (a) An averaged STM dI/dV spectrum recorded in SIN junctions at 4.2 K in an optimally doped Bi2212 sample with $T_c = 92$ K.[13] (b) ARPES spectrum obtained in a slightly overdoped Bi2212 single crystal having $T_c = 91$ K. E_F is the Fermi level.[14] (c) Typical dI/dV and $I(V)$ characteristics obtained in Bi2212 BJs. The data are recorded in a slightly overdoped Bi2212 single crystal. (d) A fine tunneling conductance obtained in a slightly overdoped Bi2212 single crystal with $T_c = 88$ K in an SIS junction. The curve has QP peaks at $V = \pm 2\Delta/e$, main humps at $\pm 4\Delta/e$, and small humps at $\pm 6\Delta/e$, where Δ is the pairing energy gap.[6]

5. Tunneling Spectroscopy in Bi2212

In this section, we discuss data obtained exclusively in *tunneling* regime, i.e. in junctions with a large normal resistance, $R_n \gg 0$. Let us start with SIN data. Figure 4a shows a conductance taken in an optimally doped Bi2212 single crystal. The conductance reflects typical features of Bi2212 spectra, namely, well-defined QP peaks, dips and humps outside the gap structure. The other feature of SIN conductances obtained in HTSC is that the height of the QP peaks is asymmetrical relatively zero bias: the QP peak at negative bias is always higher than that at positive bias (in SIS junctions, this is not the case). In SIN conductances, the humps are always situated at bias which is three times as large as that of the QP peaks, $|V_{hump}| \simeq 3\,|V_{peak}|$. Outside humps, the conductance is more or less constant.

The magnitude of a SC gap can, in fact, be derived directly from the tunneling spectrum. However, in the absence of a generally accepted model for the gap function and the DOS in cuprates, such a quantitative analysis is not straightforward. Thus, in order to compare different spectra, we calculate the gap Δ magnitude in SIN junctions as a half spacing between the QP peaks at $V = \pm\Delta/e$. In Fig. 4a, the magnitude of energy gap is about 37 meV, while the humps are situate at about

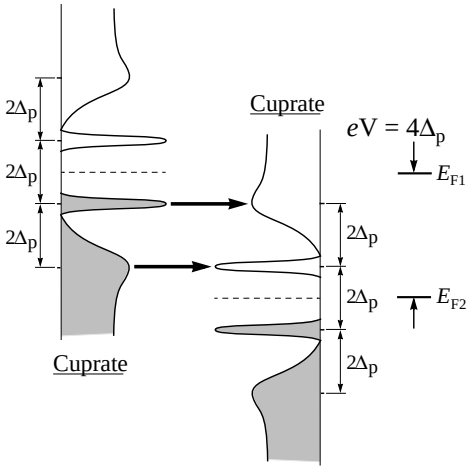

Fig. 5. Sketch of tunneling in an SIS junction of cuprates at $T = 0$, explaining the origin of the main humps in SIS conductances which appear at bias $V = \pm 4\Delta_p/e$, shown in Figs. 4c, 4d and 6. The thick arrows indicate the tunneling process. E_{F1} and E_{F2} are the Fermi levels.[6]

± 110 mV. The gap inferred from conductances obtained in the *tunneling* regime will be referred to as the pairing gap, Δ_p.

Tunneling SIN data can directly be compared with angle-resolved photoemission spectroscopy (ARPES) data. Figure 4b shows an ARPES spectrum having the same peak-dip-hump structure as the SIN conductance in Fig. 4a. In the APRES spectrum, the QP peak is situated at about 40 meV, and the hump is at about 120 meV.

Let us discuss now data obtained in SIS junctions. Figure 4c shows typical $dI(V)/dV$ and $I(V)$ tunneling characteristics for SIS junctions of Bi2212. In addition to the peak-dip-hump structure, the conductance in Fig. 4c exhibits also a peak at zero bias due to the Josephson current. In SIS conductances, the distance between the peaks is $4\Delta_p/e$, the dips are more pronounced, and the humps appears at bias $V = \pm 4\Delta_p/e$. As we shall see further, the humps in SIN conductance correspond to a normal-state gap, the tunneling PG. If so, then, in SIS spectra, the humps should be situated at bias of $V = \pm 6\Delta_p/e$, and not at $\pm 4\Delta_p/e$. As a matter of fact, there are humps in SIS spectra at bias of $\pm 6\Delta_p/e$; however, they are very weak: they can be seen in Fig. 4d. The main humps in SIS conductances are in fact the superposition of "QP peaks" and "true humps" as illustrated in Fig. 5. This is the reason why the main humps in SIS spectra are situated at bias of $\pm 4\Delta_p/e$. $I(V)$ characteristics of cuprates will be considered in detail further.

As was mentioned in Introduction, for SC in cuprates, the carrier density in CuO_2 planes, p, is the main factor. The magnitude of pairing energy gap, Δ_p, also depends on p. The dependence $\Delta_p(p)$ in Bi2212 is monotonic as shown in Fig. 6: the magnitude of Δ_p decreases as the doping level increases. Experimentally, the

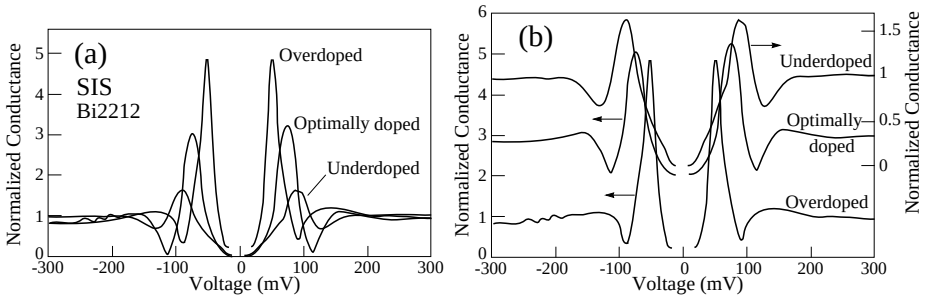

Fig. 6. (a) Tunneling conductances obtained in three Bi2212 single crystals by SIS junctions: in an underdoped Bi2212 with $T_c = 83$ K, in an optimally doped Bi2212 having $T_c = 95$ K, and in an overdoped Bi2212 with $T_c = 82$ K. In all curves, the Josephson current at zero bias has been removed. The curves are normalized at 200 mV. b) The same data as in plot (a) but the spectra are offset vertically for clarity.[15]

magnitude of Δ_p in Bi2212 linearly decreases as p increases: $\Delta_p(p) \simeq 83.7\,[1-\frac{p}{0.3}]$ (in meV).[6] In Fig. 6a, one can see that there is a correlation between the magnitude of energy gap and the height and width of QP peaks: the smaller the gap magnitude is, the higher and narrower the QP peaks are. *However*, if one normalizes the conductances by height and by gap magnitude simultaneously, they all collapse in one curve (the peaks, *not the humps*) (see Fig. 12.47 in Ref. 6).

6. Two Superconducting Gaps: Δ_c and Δ_p

Performing tunneling measurements not only in tunneling regime but also in junctions with small R_n, one will discover that there is another energy scale in cuprates. Figure 7 shows two conductances obtained within the same Bi2212 single crystal by SIS junctions. One can see that these two spectra are different: they have different shapes and different magnitudes. The upper conductance has a subgap and a zero-bias conductance peak (ZBCP) due to the Josephson current, while the other does not. Instead, the lower curve is smooth between the QP peaks and has dips and humps outside the gap structure. These differences reflect the physics of the SC state in cuprates. The upper curve is measured in a junction with low R_n, while the lower curve in a junction with high R_n. These two conductances reflect the two energy gaps, Δ_c and Δ_p, where Δ_c is the phase coherence gap. Thus, Δ_c manifests itself in tunneling spectra *exclusively* in junctions with low R_n (< 3 kΩ). In contrast, Δ_p appears in high-R_n junctions. Conductances corresponding to Δ_p always show the peak-dip-hump structure. In conductances corresponding to Δ_c, the dips are either absent or very weak. In low-R_n junctions, the ZBCP is usually large. The two energy gaps are also present in[17,6] YBCO and in electron-doped $Nd_{2-x}Ce_xCuO_4$ (NCCO).[18,6]

The two gaps have different temperature dependences. Figure 7b depicts the temperature dependence of the upper conductance in Fig. 7a, which reflects the

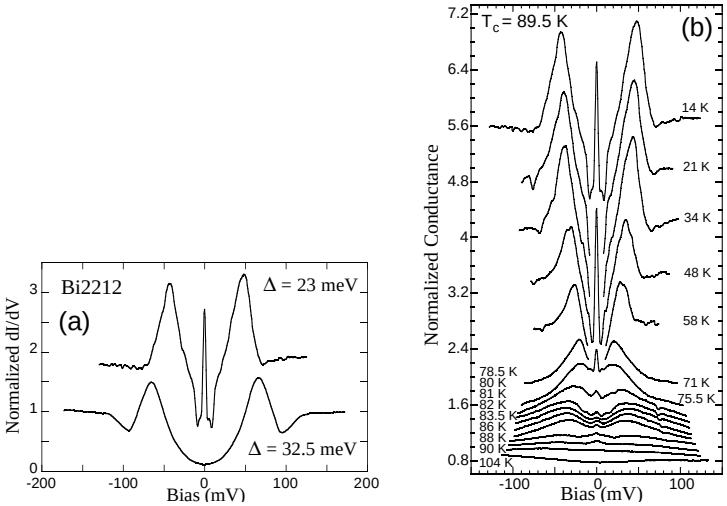

Fig. 7. (a) Two tunneling conductances obtained in a Bi2212 single crystal with $T_c = 89.5$ K ($p \simeq 0.19$) by SIS junctions.[6,8] The upper curve is offset vertically for clarity. The lower conductance is measured in a junction with $R_n \simeq 0.1$ MΩ. The upper conductance is recorded in a junction with $R_n \simeq 90$ Ω. (b) Temperature dependence of the upper conductance in plot (a). The spectra are offset vertically for clarity. In the 21 K, 34 K, 58 K and 71 K spectra, the Josephson current at zero bias has been removed for clarity.

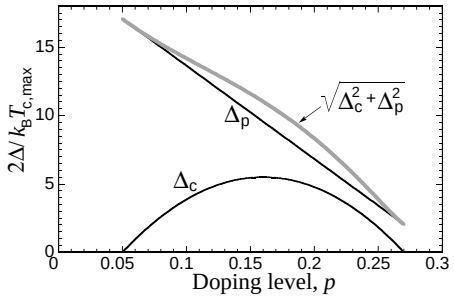

Fig. 8. Low-temperature phase diagram of SC cuprates: the pairing energy scale Δ_p is obtained in tunneling and ARPES measurements, while the phase-coherence energy scale Δ_c dominates in Andreev-reflection and penetration-depth measurements.[6,7,8,16]

$\Delta_c(T)$ dependence. In Fig. 7b, one can see that, on heating, Δ_c vanishes at T_c. As a consequence, $\Delta_c(0) \propto T_c$ as in conventional SCs: $2\Delta_c(0) = \Lambda k_B T_c$, where k_B is the Boltzmann constant, and the dependence $\Delta_c(p)$ has the shape of a dome, as shown in Fig. 8. This also means that the upper conductance in Fig. 7a, in a sense, corresponds to Andreev reflections. The coefficient Λ slightly varies in different compounds: in Bi2212 $\Lambda \simeq 5.45$; in YBCO $\Lambda \simeq 5.1$, and in $Tl_2Ba_2CuO_6$ (Tl2201)

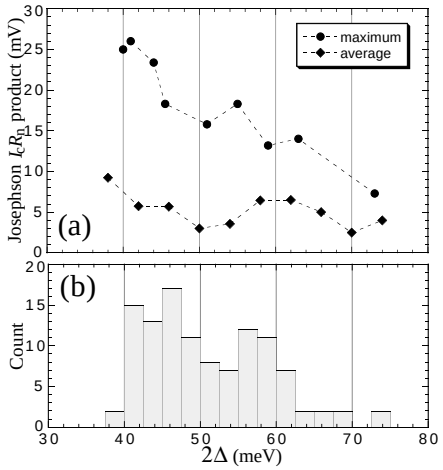

Fig. 9. (a) Maximum and average Josephson I_cR_n products as functions of the gap magnitude in 110 Bi2212 break junctions. The doping level of Bi2212 single crystals is about 0.19 ($T_c \simeq$ 87–90 K). (b) The statistics of the gap magnitude for the same 110 junctions.[19,6]

$\Lambda \simeq 5.9$.[7] The dependence $\Delta_p(T)$ will be discussed further. The fact that the Δ_p energy scale in Fig. 8 lies above the SC dome indicates that Δ_p closes *above* T_c at any doping level.

The Δ_c energy scale manifests itself in *tunneling* measurements because always $\Delta_c < \Delta_p$. *In cuprates, it is easier to excite a Cooper pair than to break it.* The excited Cooper pairs can leave the SC condensate without being broken. In conventional SCs, this is impossible. This means that the two spectra in Fig. 7a reflect two types of tunneling: the upper conductance is caused by Cooper-pair tunneling, while the lower curve by single-electron tunneling. In order to extract a single electron from the SC condensate, the minimum energy $2\sqrt{\Delta_c^2 + \Delta_p^2}$ is required. For cuprates, this energy in not deferent much from Δ_p, particularly in the underdoped region, as shown in Fig. 8. To break an uncondensed pair (e.g. on the surface), the energy $2\Delta_p$ is needed. It is important to note that ARPES studies[14] do not detect the presence of Δ_c; therefore, the Δ_c scale in Fig. 8 has exclusively the magnetic origin. There are no charges at $\Delta_c(p)$, they are "located" at the $\Delta_p(p)$ scale.

Performing tunneling measurements in junctions with different R_n, one will find that, at any fixed p, there is a distribution of gap magnitude, in a first approximation, between Δ_c and $\sqrt{\Delta_c^2 + \Delta_p^2}$. The scale of the distribution depends also on the tunneling angle into and out of the CuO_2 planes. Figure 9b shows a distribution of the tunneling gap magnitude in Bi2212 at $p = 0.19$, which is in good agreement with the values of $2\Delta_c \simeq 42$ meV, $2\Delta_p \simeq 61$ meV, and $2\sqrt{\Delta_c^2 + \Delta_p^2} \simeq 74$ meV, inferred from Fig. 8 for Bi2212 at $p = 0.19$. We turn now to the correlation between the value of the Josephson product, I_cR_n, and the magnitude of the energy gap. Figure

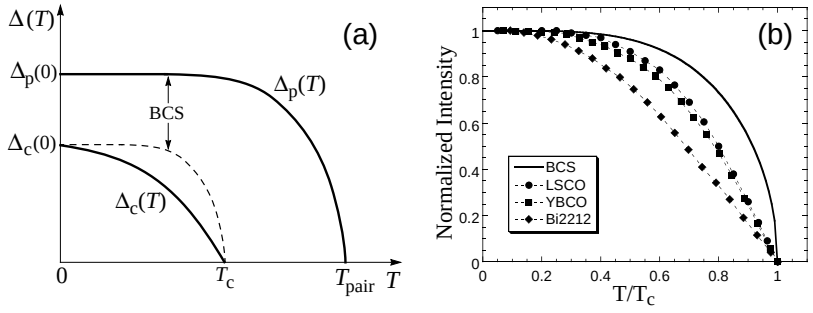

Fig. 10. (a) Typical temperature dependences of Δ_c and Δ_p in Bi2212.[6,7] The BCS temperature dependence of the gap is shown by the dashed line. The dependence $\Delta_p(T)$ is similar to the BCS one. (b) Temperature dependences of the peak intensity of the incommensurate elastic scattering in LSCO (x = 0) (T_c = 42 K) and the intensity of the magnetic resonance peak measured by INS in near optimally doped Bi2212 (T_c = 91 K) and YBCO (T_c = 92.5 K). The solid line is the BCS temperature dependence.[6,7,24,25]

9a depicts the maximum and the average I_cR_n as a function of gap magnitude in Bi2212 at $p = 0.19$. Theoretically, in low-T_c SCs, I_cR_n is proportional to Δ. In Fig. 9a, neither the average nor the maximum I_cR_n are in agreement with the proportionality $I_cR_n \propto \Delta$. This is because, in cuprates, the smaller gap Δ_c is responsible for the phase coherence, and therefore, for the value of I_cR_n. In Fig. 9a, the average product is almost flat. This is due to the fact that, in cuprates, the value of I_cR_n strongly depends on the surface quality in a junction. As a consequence, the average I_cR_n does not reflect the real I_cR_n values. However, by doing a statistical study, the real value of I_cR_n can occasionally be observed or, at least, the values close to the actual ones. In Fig. 9a, the maximum I_cR_n almost linearly depends on the gap magnitude. The maximum value of 26 mV observed at $2\Delta = 41$ meV is in good agreement with in other studies.[15] Thus, in cuprates, the phase-coherence energy scale Δ_c has the maximum Josephson strength. As a consequence, the dependence $I_cR_n(p)$ has the shape of a dome (see Fig. 12.28 in Ref. 6).

Typical temperature dependences of the two gaps are sketched in Fig. 10a. The Δ_c gap closes with increase of temperature more rapidly than that of the BCS-type gap. This can be seen in Fig. 7b. The dependence $\Delta_p(T)$ is reminiscent of the BCS one. On heating, Δ_p closes at T_{pair} which is above[20,21] T_c. This means that, between T_c and T_{pair}, Δ_p makes a contribution to the PG.[21] In Bi2212, the pairing $\Delta_p(0)$ gap is proportional to T_{pair} as[22,7] $2\Delta_p(0) \simeq 6\, k_B T_{pair}$.

7. Magnetic Origin of Δ_c

Analysis of several experimental facts indicates that the phase-coherence energy gap, Δ_c, has the magnetic origin.[6,7,17,23,24,25,26,27] In other words, the long-range phase coherence in cuprates is mediated by spin fluctuations. Consider just a few facts. The dependence $\Delta_c(T)$ shown in Fig. 10a is defined by the temperature

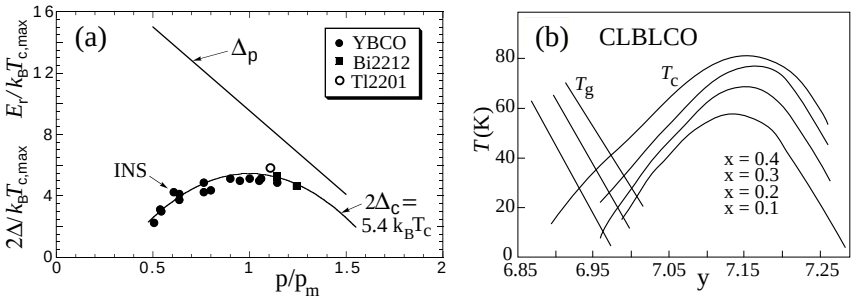

Fig. 11. (a) The phase diagram of cuprates from Fig. 8 and the energy position of the magnetic resonance peak, E_r, in Bi2212 (squares) YBCO (dots) and Tl2201 (circle) at different dopings ($p_m = 0.16$).[6,7,24,25] (b) Phase diagram of CLBLCO as a function of y at different x. The straight lines show the spin-glass-like transition temperature, T_g, for different x, determined by μSR.[26]

dependence of the intensity of spin fluctuations in cuprates. Figure 10b shows temperature dependences of the peak intensity of the incommensurate elastic scattering in LSCO and of the intensity of the commensurate resonance peak measured by INS in near optimally doped Bi2212 and YBCO. In some cuprates, the magnetic excitations in the odd (acoustic) channel undergo an abrupt sharpening on cooling through T_c. This sharp mode in the odd channel is called the magnetic resonance peak, which appears at the AF wave vector $Q = (\pi, \pi)$ below T_c. The resonance peak is a manifestation of a collective spin excitation. The AF correlations weaken in the overdoped region; however, the magnetic relaxation is still dominant in the highly overdoped region. In Fig. 10, one can see that the $\Delta_c(T)$ dependence in Fig. 10a exhibits a striking similarity with those in Fig. 10b.

At any doping level, the energy E_r, at which the resonance peak appears in INS spectra, equals to $2\Delta_c$, as shown in Fig. 11a for YBCO, Bi2212 and Tl2201. To remind, the energy $2\Delta_c$ is the condensation energy of a Cooper pair.

Recently, μSR measurements showed that the energy scale Δ_c in cuprates has the magnetic origin. At low doping level and low temperature in cuprates, there is a magnetic phase similar to spin glass. The dependence $T_g(p)$, where T_g is the transition temperature to the spin-glass-like phase, is linear as depicted in Fig. 11b for $(Ca_xLa_{1-x})(Ba_{1.75-x}La_{0.25+x})Cu_3O_y$ (CLBLCO). Decreasing x in CLBLCO, the SC dome shrinks, and the magnetic T_g scale falls down too. However, at all x, T_c and T_g remain "congruent." If one plots T_c/T_c^{max} as a function of $K(x)\Delta y$, where $\Delta y = y - 7.15$, and chooses $K(x)$ so that all T_c/T_c^{max} domes collapse to a single curve, then, T_g/T_c^{max} lines collapse to a single one too.[26] This fact indicates that the same single energy scale controls both the SC and magnetic transitions. As a consequence, Δ_c has the magnetic origin. The same scaling procedure made for LSCO, YBCO and Bi2212 gives identical results.[27]

Since the long-range phase coherence appearing at T_c couples the CuO_2 layers, Δ_c is, as a matter of fact, the c-axis energy gap. Tunneling measurements per-

formed in micron-size mesas, i.e. along the c-axis, show that the QP peaks have a temperature dependence reminiscent of $\Delta_c(T)$ in Fig. 10a and of those in Fig. 10b.[28] Bearing this fact in mind, one can draw another important conclusion from Fig. 10, namely, that the in-plane mechanism of HTSC (i.e. Δ_p) apparently has no or very little relation to magnetic interactions.

8. "Tunneling" Pseudogap above and below T_c

The PG is a depletion of the DOS above T_c. Cuprates have a connected Fermi surface that appears to be consistent with conventional band theory. At all dopings, the PG is pinned to the Fermi level and, therefore, dominates the normal-state low-energy excitations. The PG was observed for the first time in NMR measurements and, therefore, mistakenly interpreted as a spin gap. Later ARPES, tunneling, Raman, specific-heat and infrared measurements also provided evidence for a gap-like structure in electronic excitation spectra.[4] Thus, it became clear that the PG is not a spin gap but a gap to both spin and charge excitations. Alternatively, there are two spatially separated PGs: one is a spin gap and the other is a charge gap. There is a consensus on doping dependence of PG(s): the magnitude of PG(s) is large in the underdoped region and decreases as p increases.

Consider first tunneling data obtained in Bi2212 above T_c. Figure 12a shows the temperature dependence of an SIS conductance. In Fig. 12a, there is no sign indicating at what temperature the phase-coherence gap was closed. Across T_c, the spectra evolve continuously into a PG. In Fig. 12a, the 290 K conductance looks smooth; however, when enlarged vertically, it exhibits the presence of a weak PG with the magnitude of about 60 meV (see Fig. 12.23 in Ref. 6). The estimated closing temperature of this PG is about 350 K.

Figure 12b depicts the temperature dependence of another SIS conductance exclusively above T_c. In Fig. 12b, the spectra are slightly asymmetrical about zero bias. The asymmetry is caused, most likely, by the AF medium.[29] Analysis of even parts of the conductances, $G_e \equiv [G(V)+G(-V)]/2$, shows that the low-bias humps visible in the upper spectra in Fig. 12b vanish at about 115 K. The temperature dependence of zero-bias conductance has a kink in slope also near 115 K.[6] The low-bias humps were interpreted as a contribution from incoherent Cooper pairs.[21] In this case, the temperature 115 K is T_{pair} for this doping level of Bi2212. The temperature 115 K as well as the interpretation is consistent with other tunneling tests.[20] Above 115 K, the spectra in Fig. 12 reflect the presence of a normal-state PG. Knowing the values of T_{pair} and Δ_p for this doping level, one can estimate the reduce gap ratio ($2\Delta_p(0)/k_BT_{pair} \approx 6$). Running slightly ahead, it is worth to note that the temperatures 115 K and 350 K are consistent with one another (see Figs. 13c and 14). The temperature dependence of the pairing gap, $\Delta_p(T)$, is similar to the BCS one as depicted in Fig. 10a.

The normal-state PG contributes to tunneling spectra not only above T_c but also below T_c. The tunneling PG was first seen inside vortex cores.[30,6] In the underdoped

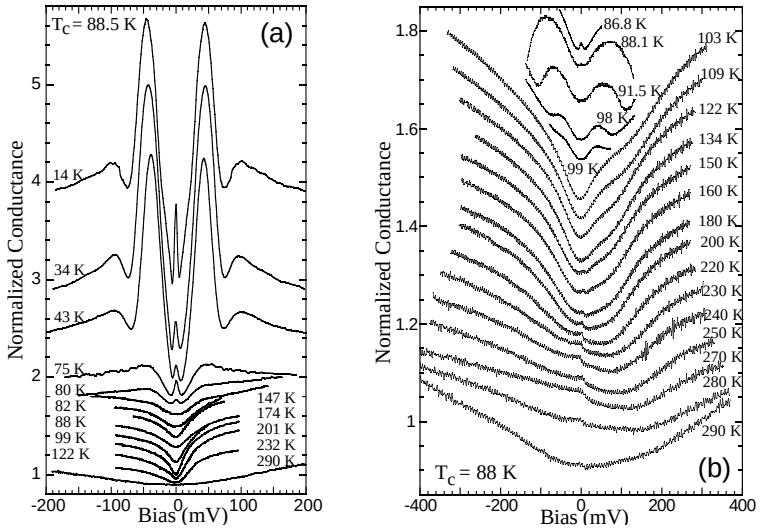

Fig. 12. (a) Temperature dependence of a conductance obtained in a Bi2212 single crystal with T_c = 88.5 K ($p \simeq 0.19$) in an SIS junction. The spectra are offset vertically for clarity. (b) Temperature dependence of a conductance above T_c, obtained in another Bi2212 with T_c = 88 K by an SIS junction. The spectra are offset vertically for clarity.[21,6] In both plots, the conductance "width" varies because of the variations of R_n with temperature.

region, where SC in cuprates is weak, the PG was directly observed even in an SIS junction. Figure 13a shows SIS $dI(V)/dV$ and $I(V)$ characteristics obtained in an underdoped Bi2212 single crystal with $T_c = 51$ K ($p \simeq 0.085$). The spectra in Fig. 13a look like usual tunneling characteristics for Bi2212. The gap magnitude of 64 meV is in good agreement with Fig. 8. The $dI(V)/dV$ and $I(V)$ characteristics depicted in Fig. 13b are obtained within the *same* single crystal as those in Fig. 13a; however, they look differently, and the gap magnitude of 130 meV is too large for a SC gap. The conductance humps in Fig.13b resemble the humps in Fig. 13a. For some reasons, the QP peaks did not develop in the conductance shown in Fig. 13b, uncovering the PG below (the sub-gap at low bias is what is left from the QP-peak contribution). From these data, one can infer that the humps in conductances are caused by a normal-state gap (in fact, the humps in Fig. 13b do not correspond *directly* to the PG—it is a product of the peak-to-PG tunneling, as shown in Fig. 5). Taking into account that these data are obtained in SIS junctions, one can conclude that $\Delta_{pg} \simeq 3\Delta_p$ as depicted in Fig. 13c [in SIN junctions, $|V_{hump}| \simeq 3\,|V_{peak}|$ (see above)]. Thus, the pairing gap appears on top of (inside) a normal-state PG. The result of mathematical subtraction between the two sets of the data presented in Figs. 13a and Fig. 13b will therefore correspond to a contribution from the SC condensate, and will be discussed below. To conclude, tunneling characteristics obtained below T_c in cuprates consist of two *independent* contributions—from the

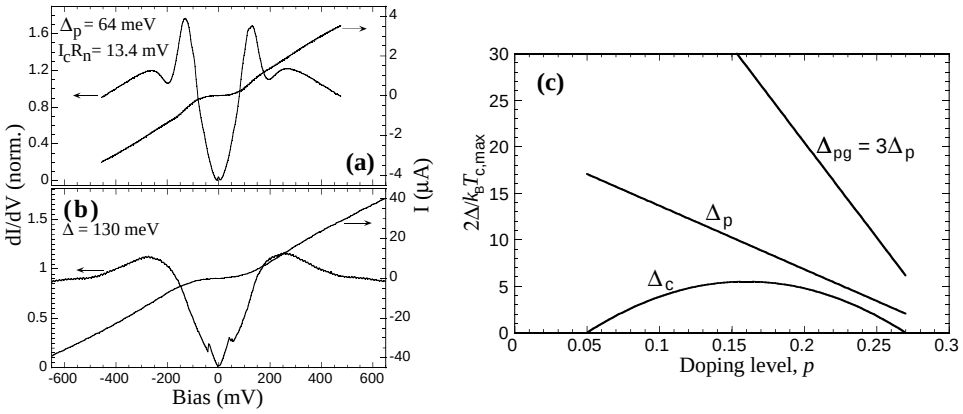

Fig. 13. (a) and (b) SIS tunneling $dI(V)/dV$ and $I(V)$ characteristics measured at 14 K within the same underdoped Bi2212 single crystal having $T_c = 51$ K. In both plots, the $dI(V)/dV$ are normalized at -400 mV. In plot (a), I_cR_n denotes the Josephson product.[6] (c) The phase diagram of SC cuprates from Fig. 8, showing also the tunneling normal-state PG, Δ_{pg}.[6,7]

SC condensate (QP peaks) and from the PG (humps at high bias). Tunneling data taken recently in micron-size mesas[28] and ARPES data[14] measured in Bi2212 at momentum near (0, π) also show that QP peaks and humps in the spectra have different origins, and humps are caused by a normal-state PG.

In the following section, it will be shown that the tunneling PG is most likely a charge gap. Analysis of tunneling and ARPES data indicates that the the *magnitude* of the tunneling PG is not affected much by cooling through T_c; however, there is a re-organization of excitations *inside* the PG (see Fig. 12.9 in Ref. 6 or Fig. 5.15 in Ref. 7). Below T_c, the SC gaps are predominant. Between T_c and T_{pair}, incoherent Cooper pairs in cuprates contribute to tunneling characteristics.

8.1. *Magnetic Normal-State Pseudogap*

The tunneling PG is not the only one in cuprates. In heat-capacity, NMR and transport measurements, the PG vanishes at $p \simeq 0.19$ (a quantum critical point in cuprates), as depicted in Fig. 14 for Bi2212. Elsewhere,[32,6,7] it was suggested that the magnetic T_{MT} and the charge ordering T_{CO} temperature scales belong to different phases; thus, they are spatially separated. Tunneling surface mapping measurements in Bi2212 show that there are patches of, at least, two different phases in CuO_2 planes.[33] What is interesting is that, in a first approximation, the two temperature scales, namely, T_{CO} and T_{MT} in Fig. 14 intersect the vertical axis in one point, at about 980 K. In the phase-separation scenario however, this fact can be naturally understood.[32,6,7] In order to plot the Δ_{pg} energy scale in Fig. 14, we assumed that $T_{CO} \simeq 3T_{pair}$ since $\Delta_{pg} \simeq 3\Delta_p$. The T_c and T_{MT} temperature scales in Fig. 14 have the magnetic origin.

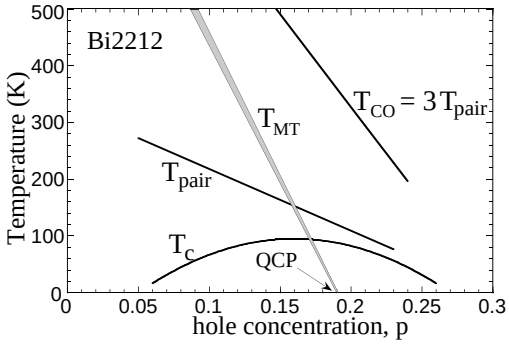

Fig. 14. Phase diagram for Bi2212 based on Fig. 13c. T_{pair} is the pairing temperature ($2\Delta_p = 6k_BT_{pair}$), T_{CO} is the PG temperature ($T_{CO} = 3T_{pair}$; CO = charge ordering), and T_{MT} is the PG temperature obtained in transport, NMR and specific-heat measurements (MT = magnetic transition).[32,6,7,31] QCP is a quantum critical point which is located in Bi2212 at $p \simeq 0.19$.

9. Measurements in Ni and Zn Doped Bi2212

By promoting or suppressing magnetic interactions in CuO_2 planes, one can test the origin of some energy scales in cuprates. One method to affect magnetic interactions in CuO_2 planes is to substitute a small amount of Cu atoms for magnetic or non-magnetic atoms. Ni and Zn are the most suitable for this task because they are situated next to Cu in the periodic table of chemical elements. Indeed, despite their similar effect on T_c (except in YBCO), Ni and Zn doped in CuO_2 planes cause very different effects on their local environment.[6,7]

Figure 15 presents three typical conductances obtained in pristine, Ni- and Zn-doped Bi2212 single crystals. What are the main changes in conductances obtained in Ni- and Zn-doped Bi2212 in respect with those taken in pure Bi2212? First, in conductances obtained in Zn-doped Bi2212, the ZBCP due to the Josephson current is usually smaller than that in Bi2212 conductances. In contrast, the ZBCP in conductances obtained in Ni-doped Bi2212 is always large. This fact indicates that the phase-coherence mechanism in cuprates has the magnetic origin. Second, the distance between humps in conductances obtained in Ni-doped Bi2212 is always smaller than that in conductances taken in pristine samples. In Zn-doped Bi2212, the distance between humps is unchanged. This fact reveals the non-magnetic origin of the "tunneling" PG, i.e. the "tunneling" PG is most likely a charge gap.

10. Anomaly in Tunneling $I(V)$ Characteristics

We now turn our attention to an anomaly in tunneling $I(V)$ characteristics obtained in cuprates. According to the Blonder-Tinkham-Klapwijk (BTK) predictions[35] for SIN junctions of conventional SCs, it is anticipated that, in the *tunneling* regime, $I(V)$ curves at high positive (low negative) bias, depending on R_n, lie somewhat below (above) normal-state curves. In conventional SCs, the BTK predictions are

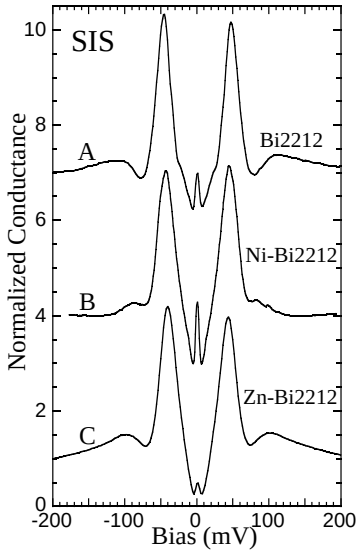

Fig. 15. Normalized conductances obtained by SIS junctions in pristine ($T_c \simeq 89$ K, $p \simeq 0.19$), Ni-doped ($T_c \simeq 75$ K) and Zn-doped ($T_c \simeq 77$ K) Bi2212, respectively. The spectra A and B are offset vertically for clarity.[34,6]

verified by tunneling experiments. As an example, Figure 2c shows typical $I(V)$ characteristics of SIN junctions for conventional SCs. In cuprates, however, the BTK theory is violated. Figure 16a depicts SIS $I(V)$ and $dI(V)/dV$ characteristics measured in Bi2212. In Fig. 16a, one can see that the $I(V)$ curve at high positive (low negative) bias passes not below (above) the straight line but far above (below) the line.[a] This fact cannot be explained by the d-wave symmetry of the order parameter. We shall refer to this positive offset in $I(V)$ curves as the anomaly.

This anomaly is a manifestation of intrinsic properties of cuprates: it appears not only in overdoped Bi2212 but also, as we shall see further, in underdoped Bi2212 as well. SIN $I(V)$ curves of Bi2212 exhibit the anomaly too, as illustrated in Fig. 16b. The anomaly is also present in $I(V)$ characteristics of YBCO, as depicted in Fig. 16e. The anomaly in $I(V)$ characteristics relates to Δ_p and, therefore, vanishes slightly above T_c. In Figs. 16c and 16d, the anomaly is absent, and a small "negative" offset from the straight line is caused by the PG. Thus, the SC condensate gives rise to an anomaly in $I(V)$ characteristics of cuprates, on top of a contribution from the PG which has a small "negative" offset from the straight line. The magnitude of "negative" offset scales with with the PG magnitude: the larger the PG magnitude is, the larger the "negative" offset is (see Fig. 12.10 in Ref. 6).

Knowing tunneling characteristics obtained deep below T_c and somewhat above

[a]The dashed line in Fig. 16a is not the normal-state curve; however, any straight line passing through zero will show that the behavior of the $I(V)$ curve in Fig. 16a deviates from the theory.[35]

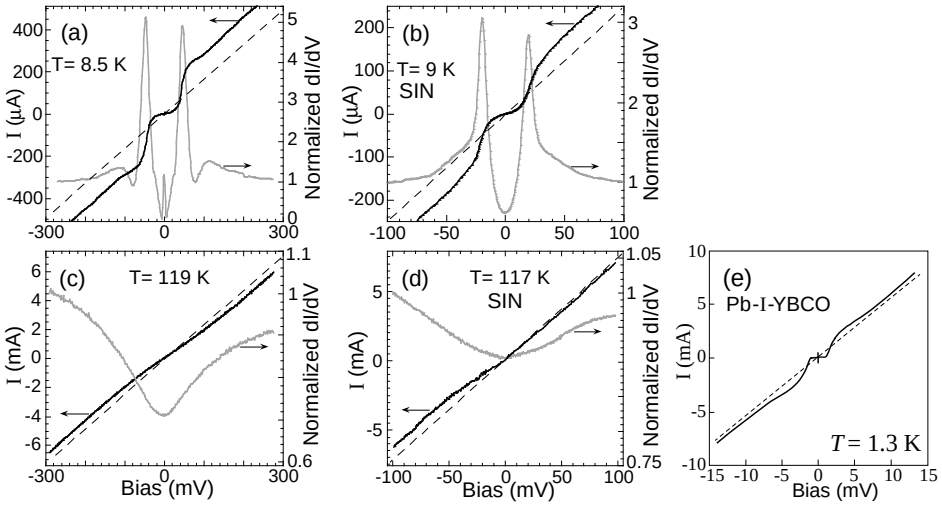

Fig. 16. (a) Tunneling $I(V)$ and $dI(V)/dV$ characteristics obtained at $T = 8.5$ K in an SIS junction of an overdoped Bi2212 single crystal with $T_c = 88$ K. (b) $I(V)$ and $dI(V)/dV$ obtained at $T = 9$ K in an SIN junction of an overdoped Bi2212 with $T_c = 87.5$ K. (c) $I(V)$ and $dI(V)/dV$ obtained at $T = 119$ K in the same SIS junction as those in plot (a). (d) $I(V)$ and $dI(V)/dV$ obtained at $T = 117$ K in the same SIN junction as those in plot (b).[36,6] (e) Tunneling $I(V)$ characteristic taken in an in-plane Pb-I-YBCO junction at 1.3 K (I = insulator).[37,6] The near optimally doped YBCO has $T_c \simeq 92$ K. In all plots, the dashed lines are parallel to the $I(V)$ curves at high bias.

T_c, and by taking the difference between the spectra, one can estimate a contribution in the tunneling spectra from the SC condensate. This procedure is equivalent to one used in INS measurements. In our case, however, such a subtraction leads only to an estimation of the contribution because by subtracting the spectra we assume that the PG crosses T_c without modification. However, as discussed above, this is not the case, particularly, at low bias.

In order to compare two sets of tunneling spectra, they should be normalized. The conductance curves can be easily normalized at high bias, as illustrated in Fig. 17a. How to normalize the corresponding $I(V)$ curves is not a trivial question. The conductance curves at high bias, thus, far away from the gap structure, are almost constant. Consequently, in a SIS junction, by normalizing two conductance curves at high bias, the equation $(dI(V)/dV)_{1,norm} \simeq (dI(V)/dV)_{2,norm}$ holds at bias $|V| \gg 2\Delta_p/e$, where e is the electron charge. By integrating the equation we have $I(V)_{1,norm} \simeq I(V)_{2,norm} + C$, where C is the constant, meaning that the corresponding $I(V)_{i,norm}$ curves are parallel to each other at high bias, as depicted in Fig. 17b.

The extracted $I(V)$ and $dI(V)/dV$ characteristics of the SC condensate appearing in SIS and SIN junctions of overdoped Bi2212 are presented in Figs. 17c and 17d, respectively. Figure 17e shows a *low-temperature* contribution of the SC condensate to tunneling spectra in *underdoped* Bi2212. At high bias, the $I(V)$ curves

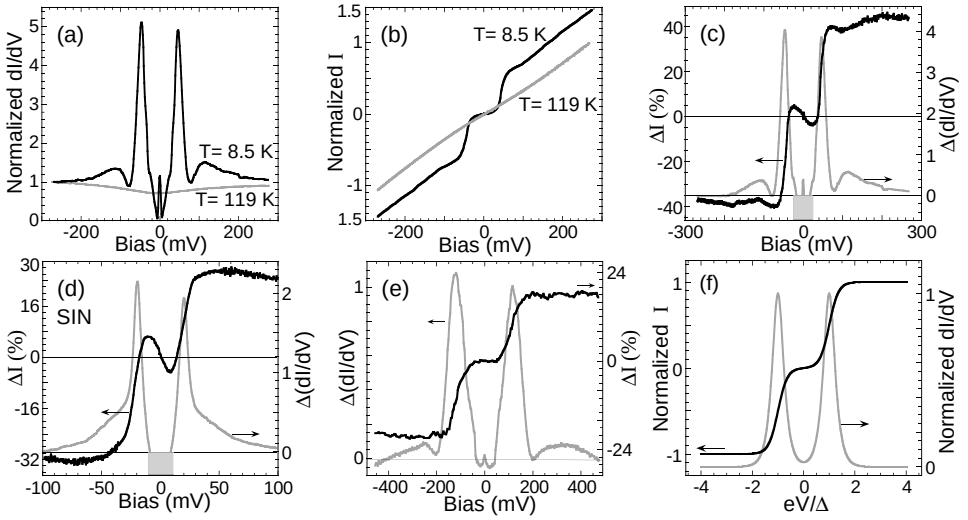

Fig. 17. (a) and (b) Normalized tunneling characteristics from Figs. 16a and 16c, which are obtained within the same Bi2212 single crystal (T_c = 88 K) at different temperatures: (a) conductances, and (b) $I(V)$ curves. In plot (b), the normalization procedure is: the normal-state curve is normalized by its value at maximum positive bias, and the other curve is adjusted to be parallel at high bias to the normalized normal-state curve (for more details, see text). (c) Differences between two conductances in plot (a) and two $I(V)$ curves in plot (b). (d) Difference between the two SIN $I(V)$ curves from Figs. 16b and 16d, normalized before subtraction as those in plot (b), and the difference between their normalized conductances. (e) Differences $(dI/dV)_a - (dI/dV)_b$ and $I_a - I_b$ between the two sets of spectra shown in Figs. 13a and 13b. The $I(V)$ curves were normalized before subtraction as those in plot (b). (f) Idealized $I(V)$ characteristic of SC condensate in an SIN junction, and its first derivative. The curves are normalized by their maximum values. In plots (c) and (d), the grey boxes cover the parts of conductances, which are below zero and have no physical meaning. In plots (c)–(e), the current difference is presented in %.[6,7,38,36]

in Figs. 17c–17e reach a plateau value. At the gap bias, they rise/fall sharply and, at low bias, the curves go to zero. In Figs. 17c and 17d, the negative slope of the $I(V)$ curves at low bias, signifying a negative differential resistance, is an artifact which a consequence of a rough estimation. Figure 17f depicts idealized $I(V)$ and $dI(V)/dV$ characteristics of the SC condensate which summarize the observed tendencies. The plateau value in the $I(V)$ curve is small in the underdoped region and increases as the doping level rises.

11. Electronic States Transfer in Cuprates

Let us consider the temperature dependence of the contributions from the SC condensate to tunneling spectra of cuprates, shown in Fig. 17f. On heating, the plateau value of $I(V)$ curves decreases, and the distance between QP peaks in conductances decreases too (see Fig. 6.5 in Ref. 6 or Fig. 6.45 in Ref. 7). The contributions vanish completely at T_{pair}. Then, a question naturally arises: where do the states of QP

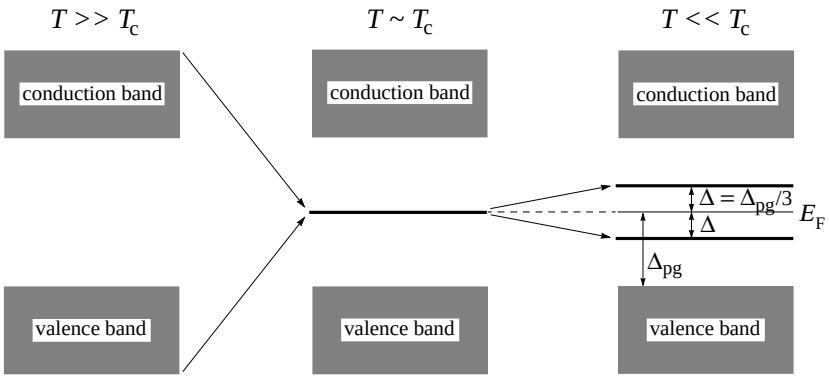

Fig. 18. Sketch illustrating the electronic states transfer in SC cuprates at different temperatures. The gap in the energy spectrum is the PG (a charge gap) which is in fact anisotropic. At $T \gg T_c$, there are no in-gap states (except thermal excitations). At $T \sim T_c$, there appear mid-gap states transfered from high energies At $T \ll T_c$, the mid-gap states split into two levels: the lower energy level corresponds to the bonding one, and the upper one to the antibonding level. At $T \ll T_c$, the magnitude of pairing gap is about one third of PG magnitude, $\Delta = \Delta_p \simeq \Delta_{pg}/3$.[6]

peaks go to? Figure 18 shows a sketch of electronic states transfer in cuprates at different temperatures, based on tunneling and ARPES data. At $T \gg T_c$, there are no in-gap states (except thermal excitations). At $T \sim T_c$, there appear mid-gap states transfered from high energies. At $T \ll T_c$, the mid-gap states split into two levels, as shown in Fig. 18. Interestingly, ARPES spectra which reflect the states exclusively above the Fermi level pass the middle step in Fig. 18 unnoticed. Thus, in ARPES spectra, the QP-peak states seem to appear directly from high energies. It is worth to remind that, in contrast to tunneling spectroscopy which probe the local DOS, ARPES probes the whole surface of a sample.

12. Origin of Cooper Pairs in Cuprates

The occurrence of in-gap states, as those in Fig. 18, is typical for system having topological solitons, for example, in polyacetylene (for a review, see Chapter 5 in Ref. 6). Moreover, the $I(V)$ and $dI(V)/dV$ characteristics of the SC condensate depicted in Fig. 17f are in good agreement with theoretical ones derived for topological solitons.[6,7,25,38] On the whole, the concept is also in agreement with the Davydov bisoliton theory of HTSC.[39,40] The bisoliton theory utilizes the concept of *bisolitons*—electron (or hole) pairs coupled in a singlet state due to a local deformation of the lattice. Thus, in the framework of the bisoliton theory, the nonlinear electron-phonon interaction is responsible for the QP pairing. A possibility for the occurrence of bipolaron SC in quasi-one-dimensional (quasi-1D) systems was suggested for the first time by Brazovskii and Kirova in 1981.[41]

Let us consider the derived characteristics for tunneling spectra obtained in a system with bisolitons. In such a system, the $I(V)$ characteristic obtained in an

SIN junction should have the following shape

$$c_n(V) = I_0 \times \left[\tanh\left(\frac{V+V_p}{V_0}\right) + \tanh\left(\frac{V-V_p}{V_0}\right)\right], \tag{6}$$

where V is voltage (bias); $V_p = \Delta_p/e$ is the peak bias, and I_0 and V_0 are constants ("c" denotes current, and "n" an SIN junction). Then, the corresponding conductance will have the shape given by

$$q_n(V) = A \times \left[\mathrm{sech}^2\left(\frac{V+V_p}{V_0}\right) + \mathrm{sech}^2\left(\frac{V-V_p}{V_0}\right)\right], \tag{7}$$

where A is a constant ("q" denotes QP peaks). In the equations, V_0 determines the width of conductance peaks. In tunneling spectra, the characteristics of bisolitons will appear on top of tunneling characteristics of other electronic states present in the system (in our case, a PG).

In SIS junctions, tunneling characteristics represent the convolution of the DOS with itself. In this particular case, the convolution cannot be resolved analytically. However, as shown elsewhere,[6] in a *first* approximation, SIS tunneling spectra obtained in a system with bisolitons can be fitted by

$$c_s(V) = I_0 \times \left[\tanh\left(\frac{V+2V_p}{V_0}\right) + \tanh\left(\frac{V-2V_p}{V_0}\right)\right], \tag{8}$$

$$q_s(V) = A \times \left[\mathrm{sech}^2\left(\frac{V+2V_p}{V_0}\right) + \mathrm{sech}^2\left(\frac{V-2V_p}{V_0}\right)\right], \tag{9}$$

where I_0, A and V_0 are constants ("s" denotes an SIS junction).

Let us use these functions to fit tunneling data. Figures 19a–19c depict tunneling $I(V)$ characteristics and the corresponding $c(V)$ fits. For simplicity, we analyze the $I(V)$ data only at positive bias. In Figs. 19b and 19c, the $c_s(V)$ and $c_n(V)$ fits, respectively, are adjusted so that the differences between the $I(V)$ curves and the fits look similar to the $I(V)$ characteristic of the PG shown in Fig. 19a. In Figs. 19b and 19c, the amplitude of the $c(V)$ functions, I_0, can be changed—this will affect only the scale but not the shape of the differences corresponding to the PG. Thus, any $I(V)$ curve measured in Bi2212 can be easily resolved into the two components if the "SC component" is interpolated by the corresponding $c(V)$ function.

The conductances and the corresponding $q(V)$ fits are depicted in Figs. 19d–19f. It is worth to remind that the $q(V)$ functions are assumed to fit exclusively the QP peaks, but not the humps. In Fig. 19, one can find good correspondence between the tunneling data and the bisoliton characteristics. The numbers used in the $c(V)$ and $q(V)$ functions shown in Fig. 19 can be found in Table 12.1 in Ref. 6.

The presence of soliton-like excitations in cuprates implies the presence of quasi-1D in CuO_2 planes. There is evidence for charge stripes in underdoped LSCO.[42] Transport properties of underdoped YBCO is quasi-1D, and there is a kind of charge ordering in undoped YBCO, e.g. CDW.[43] On the other hand, the existence of quasi-1D QPs in cuprates is not a new revelation since induced Cooper pairs on chains in YBCO are quasi-1D. This fact is already known since 1987, after the

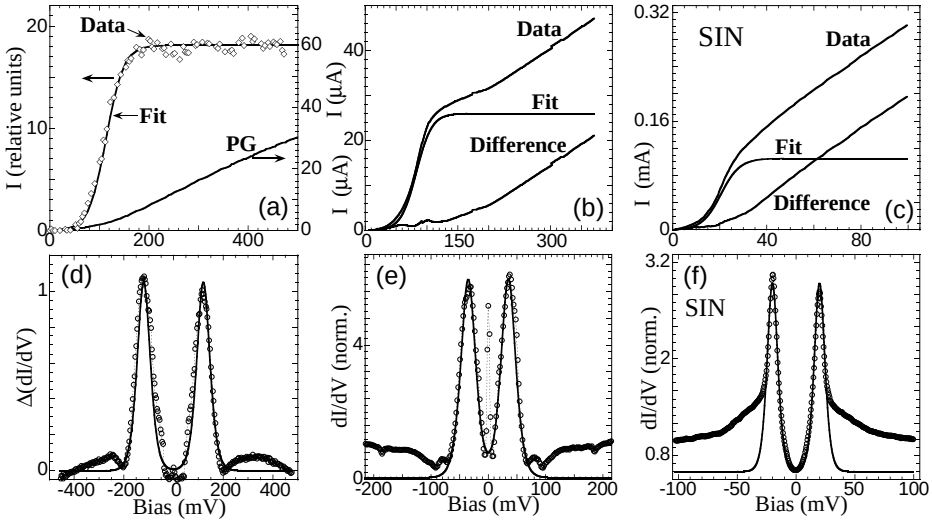

Fig. 19. (a)–(c) $I(V)$ curves obtained in Bi2212 and the $c(V)$ fits (see text). (a) SIS $I(V)$ curve (diamonds) from Fig. 17e, the $I(V)$ characteristic of PG from Fig. 13b, and the $c_s(V)$ fit. (b) SIS $I(V)$ curve obtained in an underdoped Bi2212 single crystal with $T_c = 83$ K (Fig.1 in Ref. 15), the $c_s(V)$ fit, and their difference. (c) SIN $I(V)$ curve from Fig. 16b, the $c_n(V)$ fit, and their difference. In plots (a)–(c), for simplicity, the $I(V)$ curves are presented only at positive bias. In plots (b) and (c), the Josephson current at zero bias is not shown. (d)–(f) $dI(V)/dV$ curves (circles) obtained in Bi2212 and the $q(V)$ fits (see text). (d) SIS conductance from Fig. 17e and the $q_s(V)$ fit. (e) SIS conductance measured at 15 K in a Ni-doped Bi2212 single crystal with $T_c = 75$ K the $q_s(V)$ fit. (f) SIN conductance from Fig. 16b and the $q_n(V)$ fit (see text). The spectra in plots (a), (b) and (d) are obtained in underdoped Bi2212, while in plots (c), (e) and (f) are measured in overdoped Bi2212.[6,7,25,38]

discovery of SC in YBCO. Alternatively, for example, discrete breathers which are also topological excitations can exist without the presence of quasi-1D in a system (for information about discrete breathers, see Section 13 in Chapter 5 of Ref. 6). A possibility for the existence of discrete breathers in cuprates was suggested for the first time in 1996.[44,45] Recently, defuse x-ray scattering measurements revealed the existence of lattice modulations favorable for discrete breathers.[46,47] The $4a \times 4a$ lattice modulation in cuprates may occur due to "frozen" discrete breathers.

13. Discussion

At the end, let us discuss a few important issues. First of all, let us sort out an important question related to the presence of two energy gaps in a SC. There exist at least two possibilities for a SC to have two energy gaps. First, there are two condensates in a SC, as in MgB_2, for example. In this case the two gaps are independent, and each of them belongs to one of the condensates. Second, there is only one set of Cooper pairs in a SC with a pairing gap Δ_p. They are incoherent above T_c. Due to some bosonic excitations which are different from those responsible

for the pairing, the Cooper pairs condense at T_c. Thus, for the Cooper pairs, the energy gap Δ_p is "internal," while the phase coherence gap, Δ_c, is "external." It is easy enough to discriminate these two cases. In the first case, the two gaps will appear in ARPES spectra, while in the second case, only the pairing gap (or $(\Delta_c^2 + \Delta_p^2)^{0.5}$) will be seen by APRPES. In cuprates, ARPES detects only Δ_p. This signifies that there is only one set of Cooper pairs in cuprates.

As shown above, spin fluctuations mediate the long-range phase coherence in cuprates. This means that Δ_c has the $d_{x^2-y^2}$ symmetry.[48] According to the third principle of SC presented elsewhere,[6,7] which states that *the mechanism of electron pairing and the mechanism of Cooper-pair condensation must be different*, it is most likely that the electron-phonon interaction is responsible for the QP pairing in cuprates. Analysis of some experimental facts points out in the same direction.[6,7] As a reminder, in conventional SCs, the two mechanism are different too: the electron-phonon interaction leads to the electron pairing, while the overlap of their wavefunctions is responsible for the phase coherence. What is the symmetry of Δ_p in this case in cuprates? From ARPES, it is strongly anisotropic and, *probably*, has an s-wave symmetry.

What is the main cause of the onset of SC in cuprates? After the charge-carrier doping which is absolutely necessary, the main cause of the occurrence of SC in cuprates is their **unstable lattice**. Experimentally, the lattice in cuprates is very unstable especially at low temperatures. Upon lowering the temperature, all SC cuprates undergo several structural phase transitions. In cuprates, the unstable lattice provokes a phase separation taking place in CuO_2 planes on the nanoscale ($\sim$ a few nanometers). Because of a lattice mismatch between different layers in *doped* cuprates, below a certain temperature in CuO_2 planes there appear, *at least*, two different phases which fluctuate. The doped charges prefer to join one of these phases, avoiding the other(s). By doing so, the charge presence on one phase enlarges the difference between the two phases. Thus, the phase separation is self-sustaining. Clusters containing the hole-poor phase in CuO_2 planes remain antiferromagnetically ordered (at least, up to $p \simeq 0.19$). This phase separation taking place in the normal state of cuprates on the nanoscale is the main key point for understanding of the mechanism of unconventional SC.

Spin fluctuations necessary for the phase coherence in cuprates, e.g. the so-called magnetic resonance peak, are most likely induced by dynamically fluctuating charge stripes and/or discrete breathers. Generally speaking, a charge ordering is a manifestation of self-trapped states due to the moderately strong electron-phonon interaction. Intrinsically, the charge stripes are insulating, i.e. there is a charge gap on the stripes. However, if it is the case, the presence of soliton-like excitations on the stripes makes them conducting.

In a *first* approximation, unconventional SC in cuprates can be described by a combination of two theoretical models: the bisoliton[39,40] and spin-fluctuation[49] theories. For example, the isotope effect in cuprates is in good agreement with the bisoliton theory.[5]

14. Conclusions

To summarize, analysis of the data, mainly tunneling, shows that (i) there are two SC gaps in cuprates: a pairing and a phase coherence gap. (ii) Tunneling spectra below T_c are a combination of coherent QP peaks and incoherent part from a normal-state PG. (iii) The "tunneling" normal-state PG is most likely a charge gap. (iv) However, cuprates have the second normal-state PG which is magnetic and, most likely, spatially separated from the charge PG. (v) Just above T_c, incoherent Cooper pairs contribute to the "tunneling" PG. (vi) There is a clear correlation between the magnitude of pairing gap and the magnitude of "tunneling" PG in Bi2212 ($\Delta_p \simeq \Delta_{pg}/3$). (vii) The Cooper pairs in cuprates are most likely topological excitations. They either reside on charge stripes or represent discrete breathers. (viii) The long-range phase coherence occurring at T_c is established due to spin fluctuations into CuO_2 planes. (ix) It is most likely that the nonlinear electron-phonon interaction is responsible for the QP pairing in cuprates.

More details on the mechanism of HTSC based mainly on tunneling measurements in cuprates can be found elsewhere.[6,7,50]

Acknowledgements

I would like to thank W. Y. (Yao) Liang, Peter Littlewood and Gil Lonzarich for hospitality at the Cavendish Laboratory.

References

1. H. Kamerlingh Onnes, *Commun. Phys. Lab. Univ. Leiden* **124c** (1911).
2. J. Bardeen, L. N. Cooper, and J. R. Schrieffer, *Phys. Rev.* **108** (1957) 1175.
3. J. G. Bednorz and K. A. Müller, *Z. Phys. B* **64** (1986) 189.
4. T. Timusk and B. Statt, *Rep. Prog. Phys.* **62** (1999) 61, and references therein.
5. A. Mourachkine, *Supercond. Sci. Technol.* **17** (2004) 721.
6. A. Mourachkine, *High-Temperature Superconductivity in Cuprates: The Nonlinear Mechanism and Tunneling Measurements* (Kluwer Academic Publishers, Dordrecht, 2002), pp. 56, 27, 269, 271, 221, 262, 292, 189, 210, 277, 291, 220, 64, 210, 289, 94, 99, 97, 179, 152, 140, 246.
7. A. Mourachkine, *Room-Temperature Superconductivity* (Cambridge International Science Publishing, Cambridge, 2004), pp. 208, 183, 180, 238, 206, 205, 135.
8. A. Mourachkine, cond-mat/9811284, preprint (1998).
9. M. R. Presland, J. L. Tallon, R. G. Buckley. R. S. Liu. and N. E. Flower, *Physica C* **176** (1991) 95.
10. J. L. Tallon, *Phys. Rev. B* **58** (1998) R5956.
11. S. H. Pan, E. W. Hudson, and J. C. Davis, *Appl. Phys. Lett.* **73** (1998) 2992.
12. O. Naaman, W. Teizer, and R. C. Dynes, *Phys. Rev. Lett.* **87** (2001) 097004.
13. Y. DeWilde, N. Miyakawa, P. Guptasarma, M. Iavarone, I. Ozyuzer, J. F. Zasadzinski, P. Romano, D. G. Hinks, C. Kendziora, G. W. Grabtree, and K. E. Gray, *Phys. Rev. Lett.* **80** (1998) 153.
14. A. V. Fedorov, T. Valla, P. D. Johnson, Q. Li, G. D. Gu, and N. Koshizuka, *Phys. Rev. Lett.* **82** (1999) 2179.

15. N. Miyakawa, P. Guptasarma, J. F. Zasadzinski, D. G. Hinks, and K. E. Gray, *Phys. Rev. Lett.* **80** (1998) 157.
16. G. Deutscher, *Nature* **397** (1999) 410.
17. A. Mourachkine, *Physica C* **341-348** (2000) 917.
18. A. Mourachkine, *Europhys. Lett.* **50** (2000) 663.
19. A. Mourachkine, *J. Supercond.* **14** (2001) 375.
20. T. Ekino, Y. Sezaki, and H, Fujii, *Phys. Rev. B* **60** (1999) 6916.
21. A. Mourachkine, *Europhys. Lett.* **49** (2000) 86.
22. A. Mourachkine, *J. Supercond.* **17** (2004) 771.
23. A. Mourachkine, *J. Low Temp. Phys.* **117** (1999) 401.
24. A. Mourachkine, *Europhys. Lett.* **55** (2001) 86.
25. A. Mourachkine, *Supercond. Sci. Technol.* **14** (2001) 329.
26. A. Kanigel, A. Karen, Y. Eckstein, A. Knizhnik, J. S. Lord, and A. Amato, *Phys. Rev. Lett.* **88** (2002) 137003.
27. A. Kanigel and A. Karen, *Phys. Rev. B* **68** (2003) 012507.
28. V. M. Krasnov, A. Yurgens, D. Winkler, P. Delsing, and T. Claeson, *Phys. Rev. Lett.* **84** (2000) 5860.
29. D. C. Tsui, R. E. Dietz, and L. R. Walker, *Phys. Rev. Lett.* **27** (1971) 1729.
30. Ch. Renner, B. Revaz, K. Kadowaki, I. Maggio-Aprile, and O. Fischer, *Phys. Rev. Lett.* **80** (1998) 3606.
31. J. W. Loram, J. L. Luo, J. R. Cooper, W. Y. Liang, and J. L. Tallon, *Physica C* **341-348** (2000) 831.
32. A. Mourachkine, *J. Supercond.* **17** (2004) 263.
33. K. M. Lang, V. Madhavan, J. E. Hoffman, E. W. Hudson, H. Eisaki, S. Uchida, and J. C. Davis, *Nature* **415** (2002) 412.
34. A. Mourachkine, *J. Supercond.* **13**, (2000) 101.
35. G. E. Blonder, M. Tinkham, and T. M. Klapwijk, Phys. Rev. B **25** (1982) 4515.
36. A. Mourachkine, *JETP Letters* **77** (2003) 666.
37. A. G. Sun, A. Truscott, A. S. Katz, R. C. Dynes, B. W. Veal, ans C. Gu, Phys. Rev. B **54** (1996) 6734.
38. A. Mourachkine, *Europhys. Lett.* **55** (2001) 559, and **56** (2001) 468.
39. A. S. Davydov, *Phys. Rep.* **190** (1990) 191.
40. A. S. Davydov, *Solitons in Molecular Systems* (Kluwer Academic Publishers, Dordrecht, 1991).
41. S. A. Brazovskii and N. N. Kirova, *JETP Lett.* **33** (1981) 4.
42. J. M. Tranquada, B. J. Sternlieb, J. D. Axe, Y. Nakamura, and S. Uchida, *Nature* **375** (1995) 561.
43. A. Mourachkine, *Supercond. Sci. Technol.* **13** (2000) 1378.
44. F. M. Russel and D. R. Collins, *Phys. Lett. A* **216** (1996) 197.
45. J. L. Marin, F. M. Russel, and J. C. Eilbeck, *Phys. Lett. A* **281** (2001) 21.
46. Z. Islam, X. Liu, S. K. Sinha, J. C. Lang, S. C. Moss, D. Haskel, G, Srajer, P. Wochner, D. R. Lee, D. R. Haeffner, and U. Welp, *Phys. Rev. Lett.* **93** (2004) 157008.
47. J. Strempfer, I. Zegkinoglou, U. Rütt, M. v. Zimmermann, C. Bernhard, C. T. Lin, Th. Wolf, and B. Keimer, *Phys. Rev. Lett.* **93** (2004) 157007.
48. A. Mourachkine, *Physica C* **323** (1999) 137.
49. See e.g. P. Monthoux, A. V. Balatsky, and D. Pines, *Phys. Rev. B* **46** (1992) 14803.
50. A. Mourachkine, *J. Supercond.* **14** (2001) 587.